Configurational entropy significantly influences point defect thermodynamics and diffusion in crystalline silicon

Jinping Luo [1,*] Chenyang Zhou [1] Yunjie Cheng,[1] Qihang Li,[1] Lijun Liu [1] Jack F. Douglas,[2] and Talid Sinno [3,†]

[1]*School of Energy and Power Engineering, Xi'an Jiaotong University, Xi'an, Shaanxi 710049, China*

[2]*Material Measurement Laboratory, Material Science and Engineering Division, National Institute of Standards and Technology, Gaithersburg, Maryland 20899, USA*

[3]*Department of Chemical and Biomolecular Engineering, University of Pennsylvania, Philadelphia, Pennsylvania 19104, USA*

(Received 24 March 2022; accepted 3 June 2022; published 27 June 2022)

It has long been suggested that the familiar intrinsic point defects (vacancies and self-interstitials) encountered in crystals at low temperatures (T) transform into extended domains characterized by a missing or excess atom compared with the same-sized region in the perfect crystal so that such extended defects may be viewed as dropletlike regions of enhanced or diminished density. However, the implications of such a transformation, or whether it even occurs in crystalline Si, remain uncertain. To address this fundamental problem, we consider a comprehensive thermodynamic analysis of the thermodynamics of vacancy and self-interstitial formation over a broad T range based on thermodynamic integration with a focus on entropic contributions. In cooled liquids, it is well known that the form of the intermolecular potential can greatly influence the configurational entropy S_c, and correspondingly, we analyze several empirical Si potentials to determine how the potential influences both the T dependence of S_c and the enthalpy and entropy of defect formation. We indeed find that the S_c associated with point defects increases significantly upon heating, consistent with the existence of extended defects. Moreover, each type of defect species gives a significantly different contribution to S_c at elevated T and to a qualitive difference in the T dependence of the entropy of defect formation in the extended defect regime. We discuss some potential consequences of these thermodynamic changes of defect formation on the T dependence of diffusion in heated crystals.

DOI: 10.1103/PhysRevMaterials.6.064603

I. INTRODUCTION

The thermodynamic and transport properties of intrinsic point defects, i.e., self-interstitials and vacancies, in crystalline Si have been the subject of a vast number of studies over several decades [1–11]. This persistent interest is not surprising given the central role that point defects play in establishing many of the crucial characteristics of semiconductor Si. What is surprising, however, is that, despite this collective effort, some fundamental questions remain unanswered concerning the very nature of these defects. Perhaps one of the most basic questions is whether the defects remain truly pointlike at elevated temperature or transform to diffuse defect domains or *extended defects*, thereby altering their formation and migration energetics, the configurational entropy of the crystal as a whole, and by extension, the transport properties of the material.

The notion of extended defects, proposed by Seeger and Chik [1], has been invoked to interpret certain features of Si self-diffusion measurements. In one example, apparent non-Arrhenius dependence of the self-diffusion coefficient D was attributed to a transition between point and extended defect states at an intermediate temperature [12,13]. Here, temperature-dependent thermodynamic properties for the vacancy were used to describe the effect empirically. In another study of self-diffusion [14], a very large vacancy migration energy was inferred, and once again, a transition to an extended defect state was used to reconcile this behavior with established cryogenic values [10]. The large migration energy suggested in Ref. [14] was further rationalized by Cowern *et al.* [15] in a model of point defect migration based on the physics of solid-phase epitaxy. However, others have argued that there is no need to invoke an entropic transition in defect structure. More precise measurements of self-diffusion at lower temperatures where the vacancy contribution to self-diffusion is dominant showed that the data could be fitted without the high vacancy migration energies hypothesized earlier [12,16]. Even more recent measurements [17] suggest that a single Arrhenius fit captures all self-diffusion measurements across both the self-interstitial and vacancy-dominated regimes and that earlier measurements may have been impacted by interactions with unintentional impurities or even the formation of point defect clusters [18]. Underpinning this debate are the unproven notions that (1) if a transition occurs between pointlike and extended defect conformations, it must have an obvious impact on self-diffusion, and (2) extended point defects, if they exist, must have large migration energies. The existence of extended defects thus remains unresolved.

The resolution of this fundamental problem necessitates the calculation of the configurational entropy S_c that would

*jinpingluo@xjtu.edu.cn
†talid@seas.upenn.edu

provide smoking gun evidence of these extended defects if they exist. Here, S_c is a more complex quantity to determine than the vibrational entropy of formation since it requires global sampling of the potential energy landscape (PEL) [19,20] rather than consideration of individual defect configurations. Given the relative simplicity of the calculation, the vibrational formation entropy of point defects has been studied extensively. In metals, for example, self-interstitial defects in the ground-state dumbbell, or interstitialcy, configuration [21,22] exhibit large vibrational entropies of formation, and it has been inferred that such defects lead to significant lattice softening at elevated temperatures [23,24]. Indeed, it was such calculations that led Granato *et al.* [24,25] to introduce the interstitialcy theory of simple condensed matter model of crystal melting and supercooled liquids. Moreover, recent atomistic studies have shown that vibrational anharmonicity further increases the equilibrium concentration of both self-interstitials and vacancies near the melting point of Al, Cu [23,26,27], and Fe [28,29]. Although point defect vibrational entropy in Si is somewhat less well characterized than in metals, atomistic calculations with both electronic structure and empirical methods have led to similar findings, suggesting significant vibrational entropies of formation of $\approx$4–8 k_B [5,7,30–32].

By contrast, little is known about the role of S_c in point defect formation beyond the symmetry of the respective ground states. Our previous atomistic studies demonstrated that small clusters of point defects in Si are characterized by significant S_c at high temperatures [33–37], but those works did not provide a quantitative analysis of the various entropic contributions to point defect formation free energies and their impact on diffusion. Here, we adapt the Stillinger-Weber (SW) inherent structure (IS) framework, applied to body-centered cubic (bcc) crystalline materials [22,38] but then also used extensively in the study of supercooled liquids and glasses [39–43]. This method allows for the direct estimation of the configurational entropy of point defects and more generally all (classical) entropic contributions associated with Si point defect formation. However, the application of this framework to the study of isolated point defects in a crystal is subject to certain caveats. First, only parts of the PEL that are a direct consequence of the point defect are relevant; see Fig. 1. ISs, which here correspond to local minima in the PEL introduced by a point defect, and their associated configurational entropy are localized to that defect and do not scale with the total number of atoms in the system (lower shaded band in Fig. 1). They are also not strictly part of the bulk crystal PEL which, in the absence of surfaces, can only nucleate Frenkel pairs and melt homogeneously (upper shaded band in Fig. 1) [36]. Finally, the relevant quantities for describing point defect thermodynamics are formation properties, and consequently, it is the difference between the portion of the PEL introduced by the defect and that of the perfect crystal rather than either alone that governs point defect behavior.

The study described in the remainder of this paper is based on a comparative analysis using four widely employed empirical potentials for Si: SW [44], Tersoff-94 (T94) [45], environment-dependent interatomic potential (EDIP) [46], and modified Tersoff (MOD) [47]. We show that, while the different potentials predict similar overall trends in temperature for the overall formation free energies of point defects, important qualitative discrepancies are apparent when the formation entropies are dissected into their vibrational and configurational components. These discrepancies arise from fundamental differences in how each potential describes the overall Si PEL, specifically in the density and accessibility of IS basins as temperature is increased. These findings highlight the need for future potential model regression to incorporate a more comprehensive mapping of the PEL. The remainder of this paper is structured as follows. In Sec. II, we describe the methodology for computing various thermodynamic properties as a function of temperature based on alchemical thermodynamic integration (TI). Formation properties of self-interstitials and vacancies predicted by the various potential models are presented in Sec. III. In Sec. IV, we discuss the implications of the formation properties on point defect diffusion and make a connection to Si self-diffusion. Finally, conclusions are presented in Sec. V.

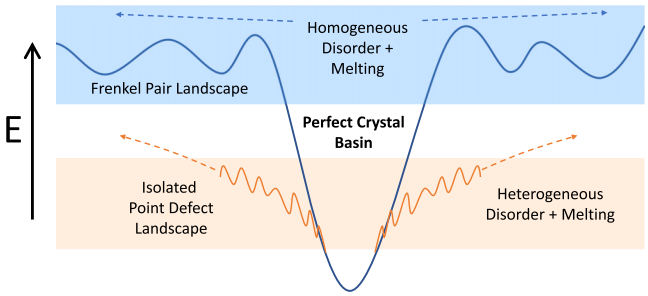

FIG. 1. Cartoon representation of the potential energy landscape (PEL) of a bulk crystal phase. Without surfaces, the crystal must nucleate its own defects, which eventually drive homogeneous melting (upper, blue-shaded band). Finite crystals bounded by surfaces can incorporate isolated point defects, which introduce their own contribution into the PEL (lower, orange-shaded band).

II. METHODOLOGY

Our overall computational strategy is based on TI to compute total free energies, a variant of which was recently demonstrated for self-interstitials in bcc Fe [28]. TI-based approaches, although computationally expensive, do not require *a priori* assumptions about the nature of entropic contributions. In this paper, we employ alchemical integration pathways using a single ideal gas particle to compute total classical point defect free energies. The free energy of the perfect crystal $G^P(T)$ is computed using the standard Frenkel-Ladd method with an Einstein crystal reference [48], while the free energy of a crystal containing a point defect is computed by gradually transforming one Si atom into an ideal-gas particle. Note that transforming a single particle into an ideal gas avoids the well-known challenges associated with performing TI across a bulk phase transformation.

The free energies of systems including a vacancy or self-interstitial, $G^V(T)$ or $G^I(T)$, respectively, are given by (see S1

in the Supplemental Material (SM) [49])

$$G^V(T) = G^P(T) + \int_0^1 \left\langle \frac{\partial U(\lambda)}{\partial \lambda} \right\rangle d\lambda + k_B T \ln \frac{\langle V \rangle_V}{N^P \Lambda^3}, \quad (1)$$

$$G^I(T) = G^P(T) - \int_0^1 \left\langle \frac{\partial U(\lambda)}{\partial \lambda} \right\rangle d\lambda - k_B T \ln \frac{\langle V \rangle_P}{N^I \Lambda^3}, \quad (2)$$

where $\langle V \rangle_P$ and $\langle V \rangle_V$ are the zero-pressure average volumes of a perfect crystal system and a vacancy containing one, respectively, at the temperature of interest, and $N^P = 512$ is the number of atoms in the host lattice (i.e., $N^I = 513$ and $N^V = 511$). Supercell sizes of 512 atoms have been shown in prior studies to be sufficiently large to fully capture the relaxation field around point defects in Si and provide converged values for formation properties [50,51]. Equations (1) and (2) are evaluated independently at every temperature. The parameter λ describes the alchemical transformation from an Si atom ($\lambda = 0$) to an ideal gas particle ($\lambda = 1$). The system potential energy $U(\lambda)$ is calculated using an empirical Si interatomic potential function for all atomic interactions except those that include the alchemical particle. The latter are computed using a soft-core modification to the potential energy function to avoid divergence in the system potential energy as the alchemical particle becomes increasingly ideal; see S2 in the SM [49]. To reduce the configuration space that must be sampled during alchemical transformations, we only consider configurations corresponding to a single defect structure that also includes the alchemical particle; see S1 in the SM [49]. All calculations are performed with molecular dynamics (MD) simulations in a cubic simulation box subject to periodic boundary conditions. All MD simulations are performed in the isothermal-isobaric (NPT) ensemble using the Nosé-Hoover thermostat and barostat implemented in the LAMMPS software package [52] with the pressure set to zero and a timestep of 1 fs.

Formation free energies are computed according to $\Delta G^{I,V}(T) = G^{I,V}(T) - \frac{N^{I,V}}{N^P} G^P(T)$. At each temperature, the average zero-pressure formation internal energy $\Delta E^{I,V}(T)$ is also computed using a similar expression. The total formation entropy is then given by $\Delta S^{I,V}(T) = [\Delta E^{I,V}(T) - \Delta G^{I,V}(T)]/T$. We also compute independently the individual contributions to the total formation entropy. The configurational entropy is calculated according to the procedure described in Refs. [53,54] (also see S4 in the SM [49]) and is given by

$$S^{I,V}_{\text{conf}}(T) = S^{I,V}_{\text{conf}}(T_0) + \int_{T_0}^{T} \frac{1}{T'} \frac{\partial \langle e^{I,V}_{\text{IS}}(T') \rangle}{\partial T'} dT', \quad (3)$$

where $\langle e^{I,V}_{\text{IS}}(T) \rangle$ is the average potential energy of ISs sampled at T. Once again, the configurational entropy of formation is obtained by subtracting the configurational entropy of the perfect crystal $S^P_{\text{conf}}(T)$—this is generally zero at temperatures up to the thermodynamic melting point except for the T94 case (see Fig. S3 in the SM [49]). The temperature T_0 is a reference temperature (typically $T \approx 300$ K) where only a single (ground state) configuration is visited, and the configurational entropy is determined only by symmetry (3 for a vacancy with D_{2d} symmetry, 6 for a ⟨110⟩-dumbbell interstitial). At each temperature T, Eq. (3) is evaluated along an isochore in which the volume is set at a value that corresponds to zero pressure at that temperature. The configurationally averaged vibrational entropy of formation is defined as the difference between the total and configurational entropy, i.e., $\Delta S^{I,V}_{\text{vib}}(T) = \Delta S^{I,V}(T) - \Delta S^{I,V}_{\text{conf}}(T)$. We also calculate the average harmonic vibrational entropy of formation at each temperature $\Delta S^{I,V}_{\text{h}}(T)$ over the sampled ISs; see S3 in the SM [49] for details. The average anharmonic vibrational entropy of formation at each temperature also may then be estimated according to $\Delta S^{I,V}_{\text{anh}}(T) = \Delta S^{I,V}_{\text{vib}}(T) - \Delta S^{I,V}_{\text{h}}(T)$.

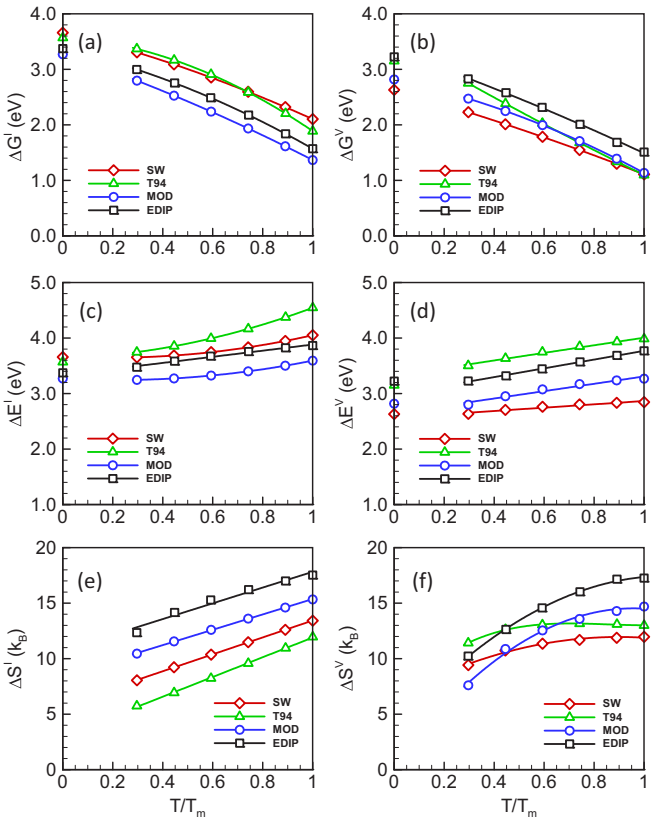

FIG. 2. Formation thermodynamic properties of isolated self-interstitials (left) and vacancies (right) as a function of temperature computed with four different empirical potentials. (a) and (b) Total formation free energy, (c) and (d) average formation energy, and (e) and (f) total defect formation entropy.

III. FORMATION THERMODYNAMICS OF POINT DEFECTS

The total formation free energies for both defect types are shown in Figs. 2(a) and 2(b) as functions of scaled temperature, $T^* \equiv T/T_m$, for all four potential models; [T_m(SW) = 1685 K, T_m(T94) = 2580 K, T_m(EDIP) = 1520 K, and T_m(MOD) = 1685 K]. For self-interstitials, the zero-temperature formation energies are clustered at $\approx 3.5 \pm 0.17$ eV, while at T_m, the average formation free energy is $\approx 2.0 \pm 0.2$ eV, corresponding to an equilibrium defect concentration of 10^{16} to 10^{18} cm^{-3}. Similar trends are observed for the vacancy: the formation energy at zero temperature is $\approx 3.0 \pm 0.2$ eV, decreasing to 1.5 ± 0.1 eV at T_m, corresponding to an equilibrium defect concentration of 10^{18} to 10^{19}

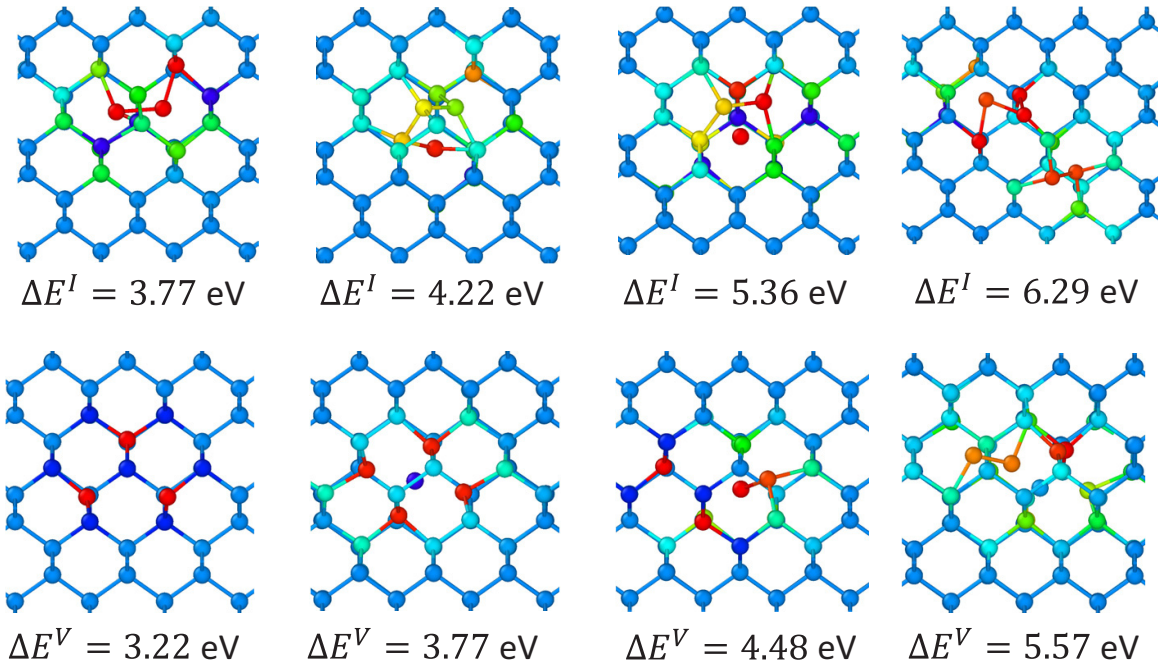

FIG. 3. Example relaxed configurations of self-interstitials (top) and vacancies (bottom) predicted by the environment-dependent interatomic potential (EDIP), along with their corresponding formation energies. The self-interstitial configuration at $\Delta E^I = 3.77$ eV corresponds to the ⟨110⟩ dumbbell, the vacancy configuration at $\Delta E^V = 3.22$ eV is the vacancy ground state, and the vacancy configuration at $\Delta E^V = 3.77$ eV is the split vacancy. Color coding represents atomic energy: red > orange > yellow > green > cyan > blue.

cm^{-3}. These concentrations are substantially higher than values employed in experimentally validated models of microdefect dynamics, which are typically ≈10^{15} to 10^{16} cm^{-3} [55–58]; we return to this discrepancy later. Also shown in Fig. 2 are the corresponding formation energies and entropies. The increase in formation energy with temperature is due to point defects assuming progressively higher energy configurations as the temperature increases, Figs. 2(c) and 2(d). This trend is driven by large total formation entropies, which averaged over the four potentials reach ≈15 k_B at the melting temperature for both point defect species. Interestingly, the total formation entropies exhibit qualitatively different temperature dependences for self-interstitials and vacancies, Figs. 2(e) and 2(f). While the total self-interstitial formation entropy rises essentially linearly with temperature (for $T^* >$ 0.3) across all four potential models, the vacancy formation entropies tend toward plateaus.

Example configurations after energy minimization of self-interstitials and vacancies are shown in Fig. 3 that correspond to several different formation energies computed with the EDIP model. Although the other potential models predict different individual configurations, the ones shown here demonstrate the general trend of increasing structural complexity as the formation energy increases that is common across all potentials.

The temperature dependence of the total formation entropy is analyzed further by decomposing it into configurational and vibrational components, as shown in Fig. 4. Generally, configurational entropy represents a significant fraction of the total formation entropy. For self-interstitials, the configurational entropy increases across the entire temperature range, and for all potentials except T94, the rate of increase is nearly constant up to the melting point. Overall, the SW potential predicts the lowest configurational entropy ∼3 $k_B T$ at $T^* = 1$, corresponding to ∼25% of the total formation entropy. At the other end of the spectrum, the T94 potential predicts rapidly increasing configurational entropy above $T^* \sim 0.6$, and by the melting point, this is the dominant contribution to the total formation entropy. The temperature dependence of the vacancy configurational entropy is qualitatively different.

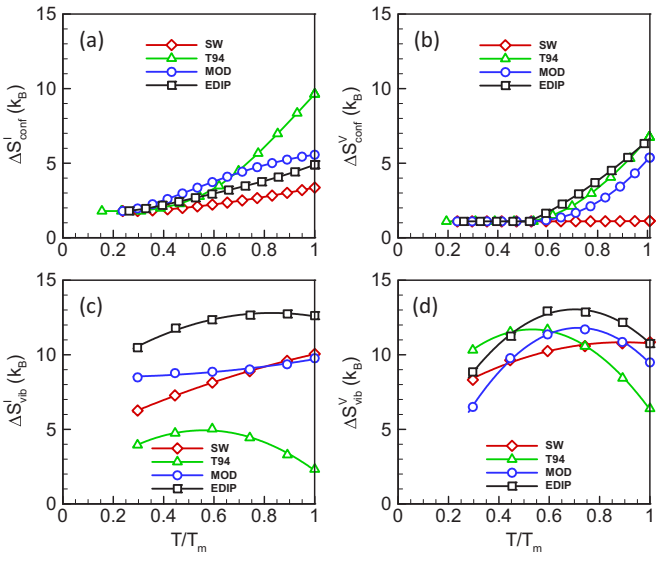

FIG. 4. Formation entropy components of isolated self-interstitials (left) and vacancies (right) as a function of temperature. (a) and (b) Configurational entropy and (c) and (d) total vibrational entropy.

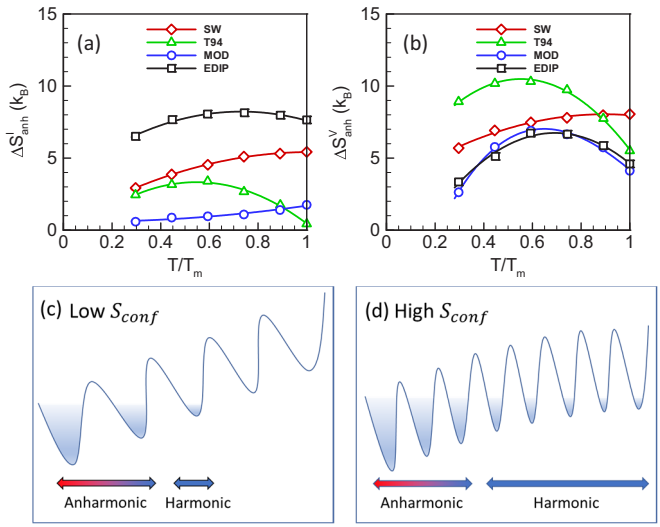

FIG. 5. Top: Anharmonic vibrational entropy of formation for (a) isolated self-interstitials and (b) vacancies as a function of temperature. Bottom: Schematic representation of collective basin occupancy in (c) low and (d) high configurational entropy settings. Blue shading in basins denotes the probability of occupancy.

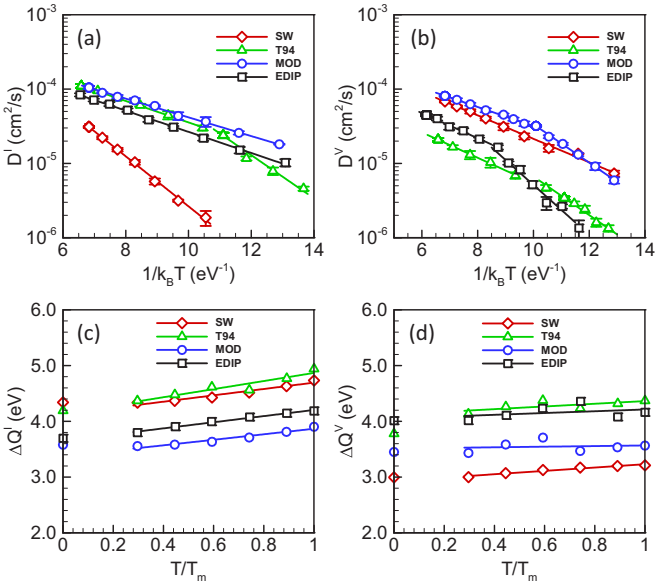

FIG. 6. Diffusivities and self-diffusion activation energies for self-interstitials (left) and vacancies (right) as a function of temperature. (a) and (b) Diffusion coefficients and (c) and (d) self-diffusion activation energies.

Vacancies exhibit a large temperature window over which the configurational entropy remains essentially zero, before suddenly and rapidly increasing at $T^* \approx 0.6$. For MOD, EDIP, and T94, vacancy configurational entropy represents >35% of the total formation entropy at $T^* = 1$. The sole exception is the SW potential which predicts zero configurational entropy (beyond symmetry) at all temperatures. This is due to the lack of accessible stable configurations beyond the ground state. The sharp onset of the vacancy configurational entropy is suggestive of the Tammann temperature [59], at which the configurational entropy and mobility at surfaces become significant. As shown in Figs. 4(c) and 4(d), the corresponding vibrational formation entropies are remarkable in that, for all cases where the configurational entropy exhibits a sufficiently large rate of increase, the vibrational formation entropy is observed to decrease with increasing temperature. Consequently, all potentials (except SW) predict maxima in the vacancy vibrational entropy of formation in the temperature interval $0.6 < T^* < 0.7$. The T94 potential also predicts similar behavior for the self-interstitial.

The origin of the peak in the vibrational entropy of formation can be traced to anharmonicity in the point defect PEL. Shown in Figs. 5(a) and 5(b) are the anharmonic contributions to the total vibrational entropies of formation for both defects. The corresponding harmonic vibrational entropies of formation, provided in Fig. S1 in the SM [49], are generally only weakly dependent on temperature. Overall, the results demonstrate that the vibrational entropy of formation is significantly impacted by anharmonicity, which on average is similar in magnitude to the harmonic contribution. In other words, the basins in the PEL generated by point defects are significantly more anharmonic than the perfect crystal basin, although the extent to which this is true is somewhat potential dependent, especially for self-interstitials. Interestingly, the anharmonic vibrational entropies exhibit the same maxima found in the total vibrational entropies—this effect is particularly notable for vacancies. A cartoon model for the nonmonotonic behavior of the anharmonic vibrational entropy of formation is shown in Figs. 5(c) and 5(d). For regions of the PEL characterized by gradual increases in configurational entropy, i.e., where basins are relatively widely spaced apart in energy, an increase in temperature leads to progressively higher energy sampling of a single or a few basins before higher energy basins are occupied, Fig. 5(c). Under these conditions, anharmonicity increases with temperature as expected. However, when basins become progressively more closely spaced in energy—corresponding to rapid increases in configurational entropy—increasing the temperature paradoxically lowers the overall anharmonicity because many basins are being sampled only in their harmonic, low-energy regions, Fig. 5(d).

IV. POINT DEFECT DIFFUSION AND Si SELF-DIFFUSION

An important question is how the preceding thermodynamic predictions impact point defect diffusion. Diffusion coefficients for self-interstitials and vacancies are shown in Figs. 6(a) and 6(b) for all four potential models as a function of temperature; see S5 in the SM [49] for details. To account for the different melting temperatures of each potential model, the temperature was rescaled to the experimental melting temperature of 1685 K, e.g., for T94, the temperature was scaled by the factor 1685/2580. Up to two distinct Arrhenius fits were defined for each case, one corresponding to a high-temperature regime and the other to a low-temperature one; the extracted migration activation energies ΔE_m are summarized in Table I. A clear distinction is apparent between diffusion that is mediated by high- and low-entropy point defect states. For all cases in which the configurational entropy is above a threshold value of $S_c \approx 3\ k_B$, the migration

TABLE I. Migration energy barriers in eV for self-interstitials and vacancies for all four empirical potential models. High-T and low-T denote different Arrhenius fit intervals—the same value is used for both intervals if a single fit is appropriate (see text for details).

	(I, high T)	(I, low T)	(V, high T)	(V, low T)
EDIP	0.32	0.32	0.38	0.81
MOD	0.31	0.31	0.30	0.63
T94	0.33	0.67	0.39	0.62
SW	0.78	0.78	0.40	0.40

barriers are tightly clustered in the range $\Delta E_m \approx 0.3$–0.4 eV. Very interestingly, this is true for both types of point defects—if enough configurations are accessible, entropically assisted diffusion proceeds with a low-energy barrier in this narrow range. Below the critical threshold of configurational entropy, point defects exist in one (or a few) low-energy configurations, and the nature of the diffusion is altered, exhibiting migration barriers in a higher range $\Delta E_m \approx 0.6$–0.8 eV. Note that it is difficult to access this regime for the MOD and EDIP self-interstitial diffusivities, and at least down to $T^* \approx 0.6$, these potentials still predict entropically assisted diffusion with a low barrier. For the vacancy cases predicted by MOD, EDIP, and T94, the transition between these two migration barrier ranges occurs suddenly at $T^* \approx 0.6$–0.7, corresponding closely to the onset of configurational entropy shown previously in Fig. 5(a). The single exception to this otherwise very consistent picture is that the SW prediction for the vacancy migration barrier, even in the absence of configurational entropy, falls in the lower range at 0.4 eV.

The impact of the predicted diffusion barriers on the self-diffusion activation energies (i.e., the sum of the formation and migration energies) is shown in Figs. 6(c) and 6(d). Although the values across different potentials are scattered over a 1 eV range, they are each essentially constant over a wide temperature interval for vacancies and only weakly temperature dependent for self-interstitials. In the latter case, the self-diffusion activation energies vary by <0.2 eV across a temperature interval of 500 °C, which would be very difficult to discern experimentally. The constant self-diffusion activation energy for vacancies arises from the competition between increasing formation energies and decreasing migration energies as the temperature increases. For self-interstitials, the weak temperature dependence is due entirely to the formation energies increasing with temperature, as most potentials predict a constant migration energy. It is also worth noting that most of the self-diffusion activation energy arises from the formation rather than migration energies, particularly at high temperature.

V. SUMMARY AND CONCLUSIONS

In summary, we show that both types of intrinsic point defects in Si exhibit significant configurational and vibrational entropy, the latter being substantially modified by anharmonicity. Our results demonstrate that an entropically driven transition to extended defect states—predicted by all models except SW—does not necessarily correspond to an obvious change in the temperature dependence of the self-diffusion behavior. We suggest that our findings therefore provide evidence that both notions can be true at the same time: (1) the self-diffusion contribution of a single defect species is approximately an Arrhenius function of temperature (i.e., exhibits a constant activation energy) over a wide temperature interval, and (2) configurational entropy drives a transition from a compact state to an extended one for both defect types. Nonetheless, it is reasonable to expect that this entropically driven transition may play an important role in various point-defect-related phenomena, such as point defect recombination (as hypothesized by Seeger and Chik [1]) and in the formation/dissolution of point defect aggregates during thermal annealing [60].

It is also worth noting that, while the configurational entropy associated with individual point defects is large and meaningfully alters the predicted formation free energies, the contribution of isolated point defects to a bulk phase configurational entropy is not significant: even at the thermodynamic melting point, the isolated point defect fractions implied by the formation free energies computed here are still $<10^{-4}$ to 10^{-5}. Consequently, finite crystalline Si samples would not be expected to melt via a point defect generation process as in metals but rather by the configurational entropy accessible through the bounding surfaces. In contrast, homogeneous melting in the absence of surfaces, which is driven by point defect generation, occurs at significantly higher temperatures ($\approx$20% above the thermodynamic melting point). Nonetheless, the nature of the temperature dependence of the vacancy configurational entropy computed in this paper and the general correspondence between homogeneous and heterogeneous melting temperatures suggests a connection between the ways that point defects and surfaces impact the PEL of a crystal.

Lastly, we address the issues of empirical potential reliability and consistency. As noted earlier, one important anomaly is that the predicted equilibrium concentrations of point defects at the Si melting point are significantly higher than accepted values by a factor of 20 to 30 averaged over the potentials [55–58]. While it is impossible to definitively attribute this error to either the ground state formation energy or to the temperature-dependent formation entropy, it is worth noting that the equilibrium concentration discrepancy amounts to <0.5 eV in their formation energy or $\sim$3–4 k_B in their formation entropy. To put these uncertainties in context, a recent summary of DFT-generated formation energies shows a scatter across studies that is at least 0.5 eV [61].

With respect to consistency across empirical potentials, the SW potential clearly predicts a qualitatively less noisy energy landscape (and lower configurational entropy) than the other models. Given the wide use of the SW and the implications with respect to the conclusions of this paper, this discrepancy deserves further analysis. Based on this paper, it is not possible to assess whether the noisier PELs predicted by T94, EDIP, and MOD are more realistic than the sparser SW one. Generally, most empirical potentials are not directly fitted to point defect thermodynamic properties, and those that do incorporate defect information tend to restrict the fitting to the (single) ground-state configuration. In this paper, we highlight the need to consider the PEL more globally in the

fitting of an empirical model, whether it be to point defect structures or something else, e.g., finite clusters or amorphous configurations. In this regard, the configurational entropy S_c may be particularly useful as a global metric for landscape quantification. A key challenge, of course, is to have this information available for potential model regression—extensive DFT-based sampling of the PEL remains extremely computationally expensive.

ACKNOWLEDGMENTS

J.L. acknowledges support from the National Natural Science Foundation of China (No. 51906188 and No. 51676154) and China Postdoctoral Science Foundation (No. 2019M653617 and No. 2020T130504). We would also like to thank Prof. Amish J. Patel for valuable discussions regarding the TI technique employed in this paper.

[1] A. Seeger and K. P. Chik, Diffusion mechanisms and point defects in silicon and germanium, Phys. Status Solidi B **29**, 455 (1968).

[2] R. Car, P. J. Kelly, A. Oshiyama, and S. T. Pantelides, Microscopic Theory of Impurity-Defect Reactions and Impurity Diffusion in Silicon, Phys. Rev. Lett. **54**, 360 (1985).

[3] T. Y. Tan and U. Gösele, Point defects, diffusion processes, and swirl defect formation in silicon, Appl. Phys. A **37**, 1 (1985).

[4] P. M. Fahey, P. B. Griffin, and J. D. Plummer, Point defects and dopant diffusion in silicon, Rev. Mod. Phys. **61**, 289 (1989).

[5] D. Maroudas and R. A. Brown, Calculation of thermodynamic and transport properties of intrinsic point defects in silicon, Phys. Rev. B **47**, 15562 (1993).

[6] G. H. Gilmer, T. Diaz de la Rubia, D. M. Stock, and M. Jaraiz, Diffusion and interactions of point defects in Silicon: Molecular dynamics simulations, Nucl. Instrum. Methods Phys. Res. B **102**, 247 (1995).

[7] T. Sinno, Z. K. Jiang, and R. A. Brown, Atomistic simulation of point defects in silicon at high temperature, Appl. Phys. Lett. **68**, 3028 (1996).

[8] H. Bracht, Diffusion mechanisms and intrinsic point-defect properties in silicon, MRS Bull. **25**, 22 (2000).

[9] S. K. Estreicher, Structure and dynamics of point defects in crystalline silicon, Phys. Status Solidi B **217**, 513 (2000).

[10] V. V. Voronkov and R. Falster, Properties of vacancies and self-interstitials in silicon deduced from crystal Growth, wafer Processing, self-diffusion and metal diffusion, Mater. Sci. Eng. B **134**, 227 (2006).

[11] P. Pichler, *Intrinsic Point Defects, Impurities, and Their Diffusion in Silicon*, Computational Microelectronics (Springer, Vienna, 2004).

[12] G. D. Watkins, The vacancy in Silicon: Identical diffusion properties at cryogenic and elevated temperatures, J. Appl. Phys. **103**, 106106 (2008).

[13] R. Kube, H. Bracht, E. Hüger, H. Schmidt, J. L. Hansen, A. N. Larsen, J. W. Ager, E. E. Haller, T. Geue, and J. Stahn, Contributions of vacancies and self-interstitials to self-diffusion in silicon under thermal equilibrium and nonequilibrium conditions, Phys. Rev. B **88**, 085206 (2013).

[14] H. Bracht, J. F. Pedersen, N. Zangenberg, A. N. Larsen, E. E. Haller, G. Lulli, and M. Posselt, Radiation Enhanced Silicon Self-Diffusion and the Silicon Vacancy at High Temperatures, Phys. Rev. Lett. **91**, 245502 (2003).

[15] N. E. B. Cowern, S. Simdyankin, C. Ahn, N. S. Bennett, J. P. Goss, J.-M. Hartmann, A. Pakfar, S. Hamm, J. Valentin, E. Napolitani, D. De Salvador, E. Bruno, and S. Mirabella, Extended Point Defects in Crystalline Materials: Ge and Si, Phys. Rev. Lett. **110**, 155501 (2013).

[16] Y. Shimizu, M. Uematsu, and K. M. Itoh, Experimental Evidence of the Vacancy-Mediated Silicon Self-Diffusion in Single-Crystalline Silicon, Phys. Rev. Lett. **98**, 095901 (2007).

[17] T. Südkamp and H. Bracht, Self-diffusion in crystalline silicon: A single diffusion activation enthalpy down to 755 °C, Phys. Rev. B **94**, 125208 (2016).

[18] D. Caliste and P. Pochet, Vacancy-Assisted Diffusion in Silicon: A Three-Temperature-Regime Model, Phys. Rev. Lett. **97**, 135901 (2006).

[19] D. J. Wales, *Energy Landscapes: Applications to Clusters, Biomolecules and Glasses* (Cambridge University Press, Cambridge, 2003).

[20] M. Goldstein, Viscous liquids and the glass transition: A potential energy barrier picture, J. Chem. Phys. **51**, 3728 (1969).

[21] P. H. Dederichs, C. Lehmann, and A. Scholz, Resonance Modes of Interstitial Atoms in fcc Metals, Phys. Rev. Lett. **31**, 1130 (1973).

[22] F. H. Stillinger and T. A. Weber, Point defects in bcc Crystals: Structures, transition Kinetics, and melting implications, J. Chem. Phys. **81**, 5095 (1984).

[23] E. V. Safonova, Y. P. Mitrofanov, R. A. Konchakov, A. Yu Vinogradov, N. P. Kobelev, and V. A. Khonik, Experimental evidence for thermal generation of interstitials in a metallic crystal near the melting temperature, J. Phys. Condens. Matter **28**, 215401 (2016).

[24] A. V. Granato, D. M. Joncich, and V. A. Khonik, Melting, thermal expansion, and the Lindemann rule for elemental substances, Appl. Phys. Lett. **97**, 171911 (2010).

[25] A. V. Granato, Interstitialcy Model for Condensed Matter States of Face-Centered-Cubic Metals, Phys. Rev. Lett. **68**, 974 (1992).

[26] A. Glensk, B. Grabowski, T. Hickel, and J. Neugebauer, Breakdown of the Arrhenius Law in Describing Vacancy Formation Energies: The Importance of Local Anharmonicity Revealed by *Ab initio* Thermodynamics, Phys. Rev. X **4**, 011018 (2014).

[27] A. S. Bochkarev, A. van Roekeghem, S. Mossa, and N. Mingo, Anharmonic thermodynamics of vacancies using a neural network potential, Phys. Rev. Materials **3**, 093803 (2019).

[28] B. Cheng and M. Ceriotti, Computing the absolute Gibbs free energy in atomistic simulations: Applications to defects in solids, Phys. Rev. B **97**, 054102 (2018).

[29] S. Chiesa, P. M. Derlet, and S. L. Dudarev, Free energy of a ⟨110⟩ dumbbell interstitial defect in bcc Fe: Harmonic and anharmonic contributions, Phys. Rev. B **79**, 214109 (2009).

[30] P. E. Blöchl, E. Smargiassi, R. Car, D. B. Laks, W. Andreoni, and S. T. Pantelides, First-Principles Calculations of Self-Diffusion Constants in Silicon, Phys. Rev. Lett. **70**, 2435 (1993).

[31] O. K. Al-Mushadani and R. J. Needs, Free-energy calculations of intrinsic point defects in silicon, Phys. Rev. B **68**, 235205 (2003).

[32] E. Rauls and T. Frauenheim, Entropy of point defects calculated within periodic boundary conditions, Phys. Rev. B **69**, 155213 (2004).

[33] S. S. Kapur, M. Prasad, J. C. Crocker, and T. Sinno, Role of configurational entropy in the thermodynamics of clusters of point defects in crystalline solids, Phys. Rev. B **72**, 014119 (2005).

[34] S. S. Kapur and T. Sinno, Entropic origins of stability in silicon interstitial clusters, Appl. Phys. Lett. **93**, 221911 (2008).

[35] T. Sinno, A bottom-up multiscale view of point-defect aggregation in silicon, J. Cryst. Growth **303**, 5 (2007).

[36] A. M. Nieves and T. Sinno, An enthalpy landscape view of homogeneous melting in crystals, J. Chem. Phys. **135**, 074504 (2011).

[37] A. M. Nieves, C. Y. Chuang, and T. Sinno, Inherent structure analysis of defect thermodynamics and melting in silicon, Mol. Simul. **38**, 659 (2012).

[38] T. A. Weber and F. H. Stillinger, Inherent structures and distribution functions for liquids that freeze into bcc crystals, J. Chem. Phys. **81**, 5089 (1984).

[39] P. G. Debenedetti and F. H. Stillinger, Supercooled liquids and the glass transition, Nature (London) **410**, 259 (2001).

[40] F. Sciortino, Potential energy landscape description of supercooled liquids and glasses, J. Stat. Mech. (2005) P05015.

[41] F. Sciortino, W. Kob, and P. Tartaglia, Thermodynamics of supercooled liquids in the inherent-structure formalism: A case study, J. Phys. Condens. Matter **12**, 6525 (2000).

[42] A. Scala, F. W. Starr, La Nave E, F. Sciortino, and H. E. Stanley, Configurational entropy and diffusivity of supercooled water, Nature (London) **406**, 166 (2000).

[43] S. Sastry, The relationship between fragility, configurational entropy and the potential energy landscape of glass-forming liquids, Nature (London) **409**, 164 (2001).

[44] F. H. Stillinger and T. A. Weber, Computer simulation of local order in condensed phases of silicon, Phys. Rev. B **31**, 5262 (1985).

[45] J. Tersoff, Chemical order in amorphous silicon carbide, Phys. Rev. B **49**, 16349 (1994).

[46] M. Z. Bazant, E. Kaxiras, and J. F. Justo, Environment-dependent interatomic potential for bulk silicon, Phys. Rev. B **56**, 8542 (1997).

[47] T. Kumagai, S. Izumi, S. Hara, and S. Sakai, Development of bond-order potentials that can reproduce the elastic constants and melting point of silicon for classical molecular dynamics simulation, Comput. Mater. Sci. **39**, 457 (2007).

[48] D. Frenkel and A. J. C. Ladd, New Monte Carlo method to compute the free energy of arbitrary solids. Application to the fcc and hcp phases of hard spheres, J. Chem. Phys. **81**, 3188 (1984).

[49] See Supplemental Material at http://link.aps.org/supplemental/10.1103/PhysRevMaterials.6.064603 for detailed derivations of free energies, softcore potential modifications, and methodology for calculating harmonic and configurational entropy.

[50] M. J. Puska, S. Pöykkö, M. Pesola, and R. M. Nieminen, Convergence of supercell calculations for point defects in semiconductors: Vacancy in silicon, Phys. Rev. B **58**, 1318 (1998).

[51] F. Corsetti and A. A. Mostofi, System-size convergence of point defect properties: The case of the silicon vacancy, Phys. Rev. B **84**, 035209 (2011).

[52] A. P. Thompson, H. M. Aktulga, R. Berger, D. S. Bolintineanu, W. M. Brown, P. S. Crozier, P. J. in't Veld, A. Kohlmeyer, S. G. Moore, T. Dac Nguyen *et al.*, LAMMPS—a flexible simulation tool for particle-based materials modeling at the atomic, meso, and continuum scales, Comput. Phys. Commun. **271**, 108171 (2022).

[53] I. Saika-Voivod, F. Sciortino, and P. H. Poole, Free energy and configurational entropy of liquid silica: Fragile-to-strong crossover and polyamorphism, Phys. Rev. E **69**, 041503 (2004).

[54] F. Sciortino, W. Kob, and P. Tartaglia, Inherent Structure Entropy of Supercooled Liquids, Phys. Rev. Lett. **83**, 3214 (1999).

[55] T. A. Frewen, T. Sinno, E. Dornberger, R. Hoelzl, W. von Ammon, and H. Bracht, Global parameterization of multiple point-defect dynamics models in silicon, J. Electrochem. Soc. **150**, G673 (2003).

[56] T. A. Frewen, T. Sinno, W. Haeckl, and W. von Ammon, A systems-based approach for generating quantitative models of microstructural evolution in silicon materials processing, Comput. Chem. Eng. **29**, 713 (2005).

[57] T. Sinno, E. Dornberger, W. von Ammon, R. A. Brown, and F. Dupret, Defect engineering of Czochralski single-crystal silicon, Mater. Sci. Eng. R Rep. **28**, 149 (2000).

[58] V. V. Voronkov and R. Falster, Parameters of intrinsic point defects in silicon based on crystal growth, wafer processing, self- and metal-diffusion, ECS Trans. **2**, 61 (2006).

[59] R. T. K. Baker, The relationship between particle motion on a graphite surface and Tammann temperature, J. Catal. **78**, 473 (1982).

[60] T. Sinno, J. Dai, and S. S. Kapur, Microscopic underpinnings of defect nucleation and growth in silicon crystal growth and wafer processing, Mater. Sci. Eng. B **159-160**, 128 (2009).

[61] G. P. Purja Pun and Y. Mishin, Optimized interatomic potential for silicon and its application to thermal stability of silicene, Phys. Rev. B **95**, 224103 (2017).